ETO family protein Mtg16 regulates the balance of dendritic cell subsets by repressing Id2

Hiyaa S. Ghosh,[1] Michele Ceribelli,[8] Ines Matos,[1] Allan Lazarovici,[6,7] Harmen J. Bussemaker,[2,6] Anna Lasorella,[3,4,5] Scott W. Hiebert,[9] Kang Liu,[1] Louis M. Staudt,[8] and Boris Reizis[1]

[1]Department of Microbiology and Immunology, [2]Center for Computational Biology and Bioinformatics, [3]Institute for Cancer Genetics, [4]Department of Pathology, and [5]Department of Pediatrics, Columbia University Medical Center and [6]Department of Biological Sciences and [7]Department of Electrical Engineering, Columbia University, New York, NY 10032
[8]Lymphoid Malignancies Branch, Center for Cancer Research, National Cancer Institute, National Institutes of Health, Bethesda, MD 20892
[9]Department of Biochemistry, Vanderbilt University School of Medicine, Nashville, TN 37232

Dendritic cells (DCs) comprise two major subsets, the interferon (IFN)-producing plasmacytoid DCs (pDCs) and antigen-presenting classical DCs (cDCs). The development of pDCs is promoted by E protein transcription factor E2-2, whereas E protein antagonist Id2 is specifically absent from pDCs. Conversely, Id2 is prominently expressed in cDCs and promotes CD8$^+$ cDC development. The mechanisms that control the balance between E and Id proteins during DC subset specification remain unknown. We found that the loss of Mtg16, a transcriptional cofactor of the ETO protein family, profoundly impaired pDC development and pDC-dependent IFN response. The residual Mtg16-deficient pDCs showed aberrant phenotype, including the expression of myeloid marker CD11b. Conversely, the development of cDC progenitors (pre-DCs) and of CD8$^+$ cDCs was enhanced. Genome-wide expression and DNA-binding analysis identified Id2 as a direct target of Mtg16. Mtg16-deficient cDC progenitors and pDCs showed aberrant induction of Id2, and the deletion of Id2 facilitated the impaired development of Mtg16-deficient pDCs. Thus, Mtg16 promotes pDC differentiation and restricts cDC development in part by repressing Id2, revealing a cell-intrinsic mechanism that controls subset balance during DC development.

CORRESPONDENCE
Boris Reizis:
bvr2101@columbia.edu

Abbreviations used: cDC, classical DC; CDP, common DC progenitor; ChIP, chromatin immunoprecipitation; ChIP-Seq, ChIP followed by sequencing; FL, fetal liver; HSC, hematopoietic stem cell; MFI, mean fluorescent intensity; MP, myeloid progenitor; pDC, plasmacytoid DC; PSAM, position-specific affinity matrix.

DCs link innate and adaptive immunity by recognizing pathogens through pattern recognition receptors such as TLRs and orchestrating antigen-specific adaptive responses (Steinman, 2012). DCs in the steady-state lymphoid tissues are represented by two main types, classical or conventional DCs (cDCs) and plasmacytoid DCs (pDCs). cDCs are specialized APCs with a characteristic dendritic morphology, high MHC class II expression, and a unique capacity for priming naive T cells. The cDCs are comprised of two main subsets: CD11b$^+$ cDCs specialized in the presentation of exogenous antigen to CD4$^+$ T cells and CD8$^+$ cDCs capable of antigen cross-presentation to cytotoxic T cells (Merad et al., 2013). The pDCs produce type 1 IFN (IFN-α/β) upon activation through nucleic acid–sensing TLRs such as TLR7 and TLR9. Unlike cDCs, pDCs lack dendrites, have low MHC class II levels, and express many lymphoid genes and markers (Liu, 2005; Reizis et al., 2011b). The three DC subsets are conserved between mice and humans, highlighting their functional importance (Haniffa et al., 2013).

Steady-state DCs in lymphoid organs develop in a common pathway characterized by the expression of and dependence on the cytokine receptor Flt3 (Geissmann et al., 2010). This pathway in the BM proceeds through myeloid progenitors (MPs) and monocyte/DC progenitors and yields a common DC progenitor (CDP) capable of producing both cDCs and pDCs (Naik et al., 2007; Onai et al., 2007). Some CDPs

The Rockefeller University Press $30.00
J. Exp. Med. 2014 Vol. 211 No. 8 1623-1635
www.jem.org/cgi/doi/10.1084/jem.20132121

The Journal of Experimental Medicine

(such as a recently described CD115$^-$ CDP subset [Onai et al., 2013]) and possibly other lymphoid-related progenitors (Sathe et al., 2013) give rise to pDCs, which complete their differentiation in the BM. Other CDPs differentiate into restricted cDC progenitors (pre-DCs), which migrate from the BM into peripheral lymphoid organs and generate both CD11b$^+$ and CD8$^+$ cDCs (Naik et al., 2006; Liu et al., 2009). Thus, developing DC progenitors face two major cell fate choices, i.e., between pDC and cDC lineages and subsequently between the two cDC subsets. Several transcription factors were shown to facilitate general DC development (e.g., Irf8 and PU.1) or the differentiation of particular DC subsets (e.g., Batf3 in CD8$^+$ cDCs; Satpathy et al., 2012b). However, the regulation of DC progenitor commitment at the main lineage bifurcation points remains poorly understood.

One important determinant of DC subset specification is the activity of E protein transcription factors. The three mammalian E proteins (E2A, HEB, and E2-2) bind a canonical DNA sequence called E-box (CANNTG) as homo- or heterodimers, as well as recruit additional cofactors to regulate transcription (Murre, 2005; Kee, 2009). The activity of E proteins is antagonized by Id proteins (Id1–Id4) that heterodimerize with E proteins and prevent them from binding to DNA. The balance between E protein and Id protein activity dictates major cell fate choices in immune system development, including the choice between B and innate lymphoid cells in the BM (Boos et al., 2007) and between CD4$^+$ and CD8$^+$ T cells in the thymus (Jones-Mason et al., 2012). Within the DC lineage, E protein E2-2 is preferentially expressed in pDCs and is required for pDC development and maintenance (Cisse et al., 2008; Nagasawa et al., 2008; Ghosh et al., 2010). Conversely, E protein inhibitor Id2 is abundantly expressed in cDCs but is absent from pDCs, and overexpression of Id2 or Id3 inhibits pDC development in vitro (Spits et al., 2000; Ginhoux et al., 2009). Moreover, Id2-deficient animals lack CD8$^+$ cDCs (Hacker et al., 2003), which express the highest levels of Id2 among all immune cells (Jackson et al., 2011). These data suggest that the net E protein activity is a key determinant of lineage allocation in DC development, with high levels of E2-2 or Id2 favoring pDC or CD8$^+$ cDC development, respectively. However, the regulation of Id2 expression and particularly of its selective repression in pDCs and B cells is poorly understood.

ETO proteins comprise a family of transcriptional cofactors that includes three members, MTG8 (ETO1, RUNX1T1), MTG16 (ETO2, CBFA2T3), and MTGR1 (CBFA2T2). In-frame fusions of ETO proteins with DNA-binding factors such as RUNX1 (AML1, CBFA2) are frequently found in leukemia. It has been shown that both native ETO proteins and leukemogenic AML1-ETO fusion can bind to E proteins and inhibit their transactivation capacity by displacing coactivators and inducing repressive chromatin modifications (Zhang et al., 2004; Guo et al., 2009). However, the physiological role of ETO proteins in immune system development and in the regulation of E protein activity remains unclear. The loss of ETO protein Mtg16 impairs hematopoietic stem cell (HSC) function, erythropoiesis, and lymphocyte development (Chyla et al., 2008; Hunt et al., 2011; Fischer et al., 2012). Notably, these phenotypes manifest primarily in competitive settings or after stress, and it is unclear whether any of them is related to E protein activity. Although a prominent expression of Mtg16 in the DC lineage has been noted recently (Miller et al., 2012), the role of this or other ETO proteins in DC development has not been explored.

Here we report that the loss of ETO protein Mtg16 impaired the differentiation and functionality of pDCs, whereas the numbers of CD8$^+$ cDCs were increased. The defect in pDC development was associated with aberrant induction of Id2 and could be ameliorated by Id2 deletion. These data identify Mtg16 as a cell-intrinsic regulator of DC development, which promotes pDC and restricts cDC differentiation. They further suggest an unexpected positive role of ETO proteins in E protein activity, in part through the repression of Id2.

RESULTS

Mtg16 promotes pDC development and function

Given the prominent expression of ETO protein Mtg16 in DCs, we analyzed the DC compartment of *Mtg16*$^{-/-}$ mice. Because Mtg16-null pDCs have aberrant surface phenotype (see below), they were defined using a combination of surface markers and broad gates to allow for marker level variation (Fig. S1). We further defined pDCs using two pDC-specific markers, Bst2 (which was reduced on Mtg16-null pDCs) or SiglecH (which was unaffected). Either definition revealed a several-fold decrease of pDC population in the BM and spleen of *Mtg16*$^{-/-}$ mice (Fig. 1, A and B). Furthermore, Mtg16-null pDCs showed reduced levels of many characteristic surface markers, including Bst2, B220, Ly6c, and MHC class II, and a nearly complete absence of CD4 and Ccr9 (Fig. 1 C). Conversely, Mtg16-null pDCs expressed myeloid marker CD11b, which is normally absent from the pDC lineage (Fig. 1 D). The induction of CD11b was prominent (approaching the levels of monocytes and CD11b$^+$ cDCs) and specific for pDCs versus other CD11b$^-$ cells (Fig. 1 D). Thus, Mtg16-deficient pDCs are both reduced in numbers and have an aberrant surface phenotype, as described in several models including *Ikaros*$^{L/L}$ (Allman et al., 2006), *E2-2*$^{+/-}$ (Cisse et al., 2008) and *Runx2*$^{-/-}$ (Sawai et al., 2013) mice.

Consistent with the reduction of pDCs, the production of IFN-α in response to Tlr9 ligand unmethylated CpG oligonucleotides (CpG) was reduced in cultures of *Mtg16*$^{-/-}$ BM and spleen cells (Fig. 1 E). A minor (~1.5-fold) but significant reduction was also observed in sorted Mtg16-null pDCs, suggesting an additional functional defect (Fig. 1 E). Similarly, intracellular staining showed an ~1.5-fold reduction of IFN-α–producing cells within the pDC population (not depicted). We then tested CpG-induced production of serum IFN-α, which serves as a specific readout of pDC activity in vivo (Reizis et al., 2011a). Strikingly, *Mtg16*$^{-/-}$ mice failed to produce IFN-α after CpG challenge, although they showed efficient IFN-α response to non-pDC–specific ligand poly-I:C (Fig. 1 F). The complete lack of CpG-induced IFN-α response likely

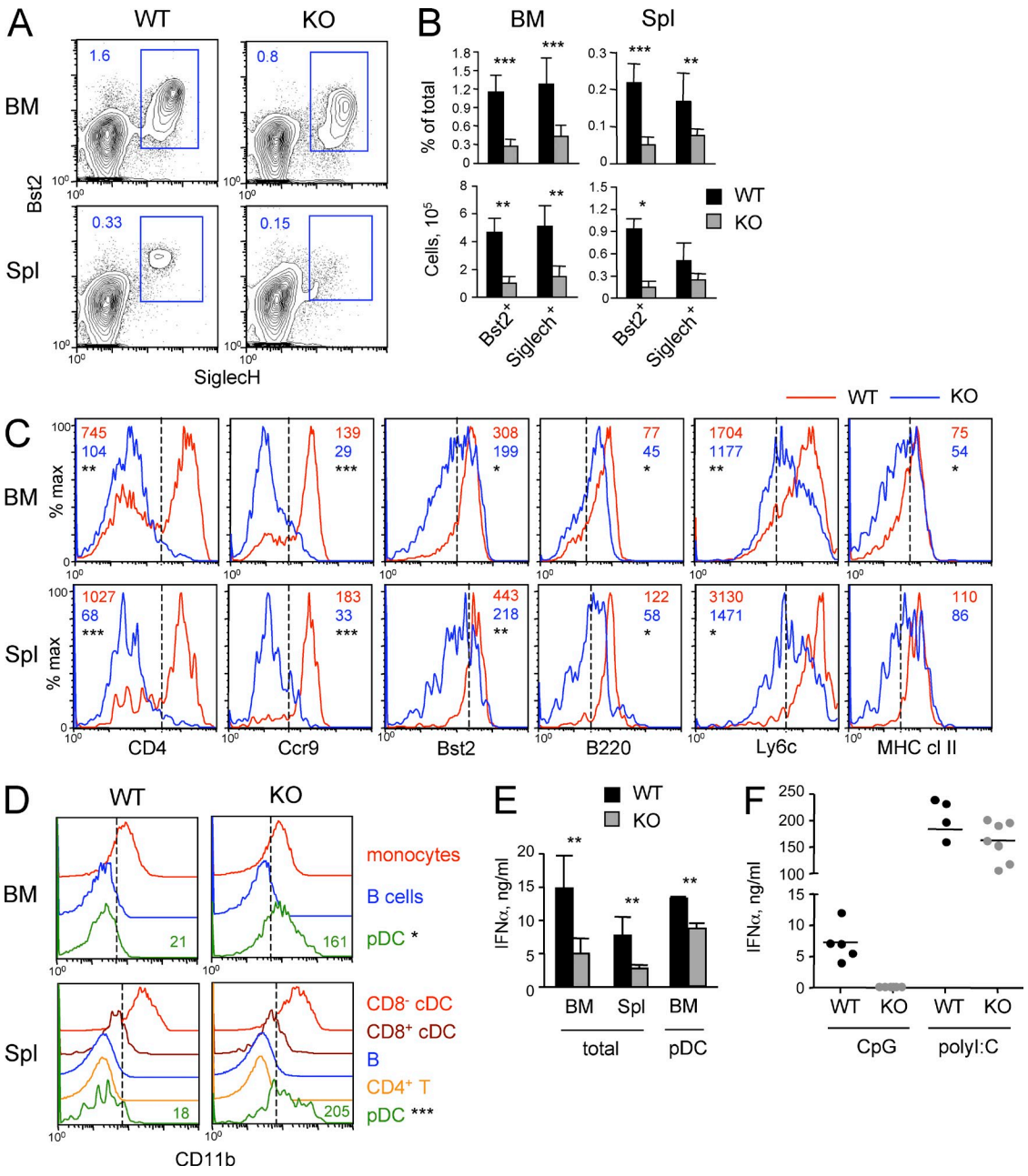

Figure 1. Impaired pDC development and function in Mtg16-deficient mice. (A) The pDC population in *Mtg16*$^{-/-}$ (KO) mice and WT controls was defined by surface staining. Shown are staining profiles of gated CD11c$^+$ cells from the BM or spleen (Spl), with the SiglecH$^+$ Bst2$^+$ pDC population and its fraction among total cells indicated (representative of six animals per group). (B) The fraction and absolute numbers of pDCs in the BM and spleen of WT and KO animals (mean ± SD of six animals pooled from two independent experiments). The pDC population was defined using a combination of markers B220, Ly6c, CD11c, and either Bst2 or SiglecH. Statistical significance is indicated by asterisks as described in the Materials and methods. (C) Surface phenotype of BM and splenic pDCs from KO and WT mice. Shown are histograms of pDCs stained for the indicated markers and gated on a combination of at least three markers distinct from the one shown. Mean fluorescent intensities (MFIs) averaged from three animals from one experiment are shown; data are representative of three independent experiments. Thresholds of positive staining (dashed lines) were established using directly conjugated isotype controls. (D) The expression of CD11b in pDCs from KO and WT mice. Data are presented as above for gated pDCs and other indicated cell types, with MFIs for pDCs shown (averaged from three animals per group, representative of three independent experiments). (E) IFN-α production by KO or WT cells in vitro. Total BM cells or splenocytes or sorted BM pDCs were cultured with CpG, and IFN-α in the supernatants was measured by ELISA. Data represent mean ± SD of cultured cells independently isolated or sorted from three individual animals per genotype. (F) IFN-α production after in vivo challenge with CpG DNA. Serum IFN-α concentrations in KO mice or WT controls were measured 6 h after CpG injection or 12 h after poly-I:C injection. Values in individual mice (circles) and group means (lines) are shown; the difference in CpG response is significant using Wilcoxon signed-rank test. Data are from a single experiment representative of two independent experiments. No IFN-α was detected in naive mice of any genotype (not depicted). *, P ≤ 0.05; **, P ≤ 0.005; ***, P ≤ 0.0005.

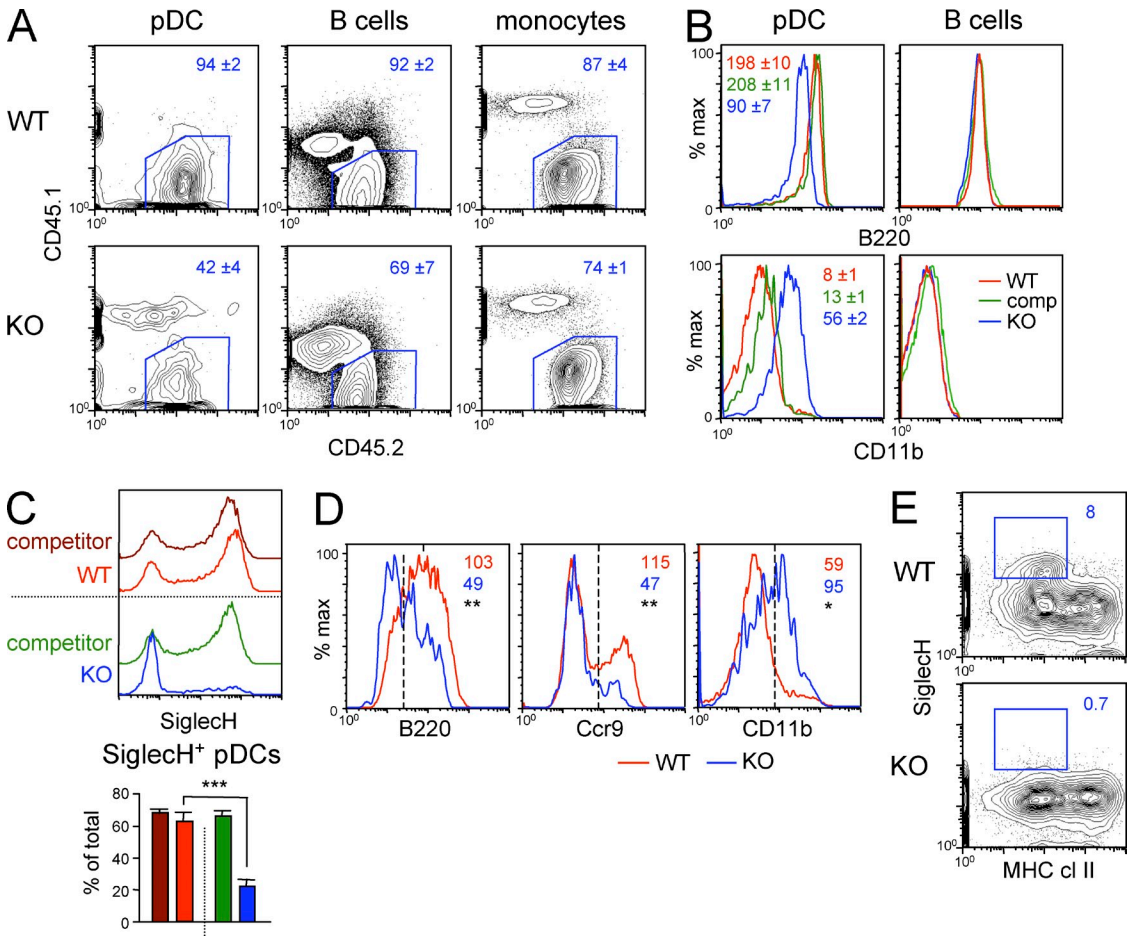

Figure 2. The cell-intrinsic role of Mtg16 in pDC development. (A) Chimeras reconstituted with 95% CD45.2 donor *Mtg16*$^{-/-}$ (KO) or WT BM and 5% CD45.1 competitor BM were analyzed at 5 wk after reconstitution. Shown is the fraction of donor-derived CD45.1$^-$ CD45.2$^+$ cells among the indicated gated cell types in the BM (mean ± range of two animals from a single experiment representative of two experiments). (B) Expression of the indicated surface markers in pDCs and B cells from the BM of competitive chimeras described above. Histograms of expression in CD45.1$^+$ competitor cells and CD45.2$^+$ WT or KO donor cells are shown; MFIs represent mean ± range of two animals from a single experiment representative of two experiments. (C) CD45.2 *Mtg16*$^{-/-}$ (KO) or WT BM cells were mixed 50:50% with CD45.1 competitor BM cells and cultured with Flt3L. Shown is representative staining for pDC marker SiglecH of WT or KO cells along with competitor cells from the same culture. The fraction of SiglecH$^+$ pDCs among total cells of the respective origin is indicated (mean ± SD of cultures from three individual animals per genotype analyzed in one experiment, representative of two experiments). (D) Surface phenotype of KO or WT donor-derived pDCs in competitive Flt3L cultures from C. Shown is expression of the indicated markers in CD45.2$^+$ CD11c$^+$ SiglecH$^+$ pDCs; thresholds of positive staining are indicated with dashed lines. MFIs represent mean values of cultures from three individual animals per genotype in a single experiment representative of two experiments. (E) Flt3$^+$ DC progenitors were sorted from the BM pooled from eight KO or five WT animals and cultured with Flt3L. Shown is the staining of total cultured cells, with the SiglecH$^+$ MHC class II$^-$ pDC fraction indicated (results from one experiment representative of two experiments). *, P ≤ 0.05; **, P ≤ 0.005; ***, P ≤ 0.0005.

reflects the reduced number and IFN-producing capacity of Mtg16-null pDCs, as well as additional defects of their in vivo function such as impaired migration (Asselin-Paturel et al., 2005). Indeed, impaired IFN production by pDCs in vivo but not in vitro has been recently documented in very young animals (Belnoue et al., 2013). Collectively, the loss of Mtg16 results in reduced pDC development, aberrant differentiation, and impaired pDC-dependent immune response.

Mtg16 acts in a pDC-intrinsic manner

To test whether the function of Mtg16 in pDCs is cell intrinsic, we analyzed mice that were competitively reconstituted with WT and *Mtg16*$^{-/-}$ BM. Quantitative analysis of pDC development was precluded by the competitive disadvantage of *Mtg16*$^{-/-}$ HSCs (Fischer et al., 2012) and rapid disappearance of their progeny in chimeras reconstituted at 50:50% ratio (not depicted). We therefore reconstituted CD45.1 recipients with 95% CD45.2 donor and 5% CD45.1 competitor BM. Control BM faithfully reconstituted to ∼90–95% at all time points, whereas Mtg16-null donor contribution was evident at 5 wk but became barely detectable by 8 wk (Fig. 2 A and not depicted). At 5 wk, *Mtg16*$^{-/-}$ BM yielded ∼70% chimerism in B cells and monocytes, but only ∼40% in pDCs (Fig. 2 A). Furthermore, the resulting Mtg16-null pDCs showed the same

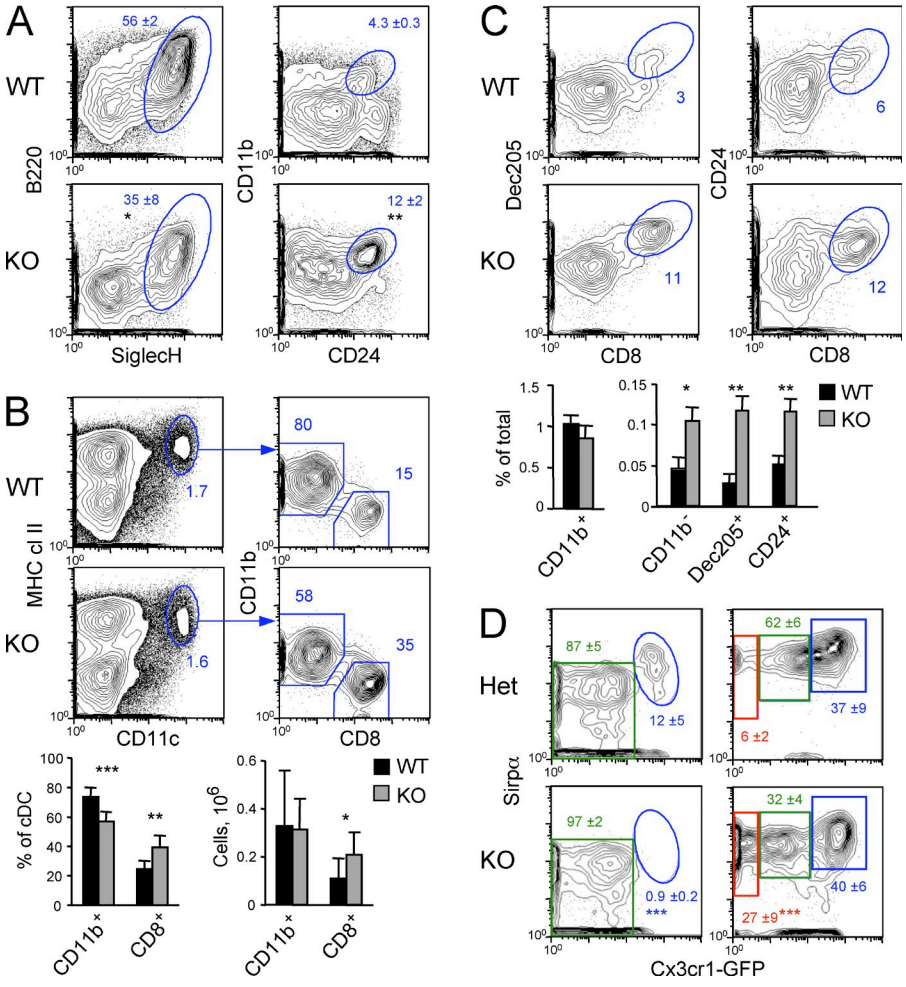

Figure 3. Enhanced cDC differentiation in Mtg16-deficient mice. (A) DC development in Flt3L-supplemented BM cultures from *Mtg16*$^{-/-}$ (KO) or WT animals. Shown are staining profiles of gated CD11c^{+} cells on day 7 of culture, highlighting SiglecH^{+} B220^{+} pDCs (left) or CD11b^{+} CD24^{+} cells that may represent CD8^{+}-like cDCs (right). The fractions of these cells are indicated (mean ± SD of cultures from three animals per genotype, representative of three experiments). (B) The cDC population in the spleens of KO and WT animals. Shown are representative profiles of total splenocytes with the CD11c^{hi} MHC II^{hi} cDC fraction and its CD11b^{+} and CD8^{+} subsets highlighted. The fraction among total splenic cDCs and absolute numbers of CD11b^{+} and CD8^{+} cDC subsets are shown (mean ± SD of five to seven animals pooled from three experiments). (C) Splenocytes from KO and WT animals were stained with additional markers of CD8^{+} cDCs. Shown are the population of Dec205^{+} or CD24^{+} CD8^{+} cDCs within the gated cDCs and the fraction of these subsets among total splenocytes (mean ± SD of three animals, representative of three experiments). (D) The distribution of cDC subsets defined by the expression of *Cx3cr1*-GFP reporter. Shown are representative profiles of GFP expression in gated CD8^{+} and CD11b^{+} cDC subsets from *Mtg16*$^{+/-}$ (Het) or *Mtg16*$^{-/-}$ (KO) mice crossed to *Cx3cr1*-GFP reporter, with the frequencies of GFP-based subpopulations among the respective cDC subset indicated (mean ± SD of three animals from one experiment representative of two experiments). *, P ≤ 0.05; **, P ≤ 0.005; ***, P ≤ 0.0005.

reduction of B220 and expression of CD11b (Fig. 2 B). This aberrant phenotype was observed in Mtg16-null but not control or competitor pDCs and was specific for pDCs versus B cells (Fig. 2 B). To confirm the pDC-intrinsic activity of Mtg16 independently of the HSC defect, we established Flt3L-supplemented cultures of total WT or *Mtg16*$^{-/-}$ BM cells mixed 50:50% with CD45.1 competitor BM. We observed an approximately threefold reduction in the fraction of Mtg16-null pDCs (Fig. 2 C), which had the same aberrant phenotype as ex vivo pDCs (Fig. 2 D). Finally, we sorted Flt3^{+} DC progenitors from control and *Mtg16*$^{-/-}$ BM and cultured them with Flt3L. Although MHC II^{+} cDCs were produced in both cultures, the MHC II^{-} SiglecH^{+} pDC population was absent from Mtg16-null cultures (Fig. 2 E). Altogether, these data suggest a cell-intrinsic requirement for Mtg16 in pDC development and differentiation.

Mtg16 restricts the differentiation of cDCs

Noncompetitive cultures of *Mtg16*$^{-/-}$ BM showed the expected reduction of pDCs fraction; in addition, we observed a threefold increase in CD11b^{+} CD24^{+} cells that may correspond to CD8^{+} cDC-like cells (Naik et al., 2005) or their precursors (Fig. 3 A). We therefore tested whether impaired pDC development in *Mtg16*$^{-/-}$ mice is associated with a shift toward the alternative cDC cell fate. The analysis of splenic cDC compartment revealed an increased fraction of CD8^{+} cDCs, reflecting an approximately twofold increase in their absolute numbers (Fig. 3 B). Staining for additional CD8^{+} cDC markers Dec205 and CD24 confirmed the increased fraction of CD8^{+} cDCs in the spleen (Fig. 3 C).

Besides the canonical pre-DC–derived CD8^{+} cDCs, the CD8^{+} DC population includes a subset that is related to pDCs and requires E2-2 for development (Bar-On et al., 2010). We therefore crossed *Mtg16*$^{-/-}$ mice to the *Cx3cr1*-GFP reporter, which distinguishes the two subsets as GFP^{-} and GFP^{hi}, respectively. The CD8^{+} cDC population in *Mtg16*$^{-/-}$ mice consisted exclusively of the GFP^{-} subset, whereas GFP^{hi} CD8^{+} cDCs were virtually absent (Fig. 3 D). Thus, the loss of Mtg16 blocks the development of "pDC-like" but not of the canonical CD8^{+} cDCs. We also noticed that CD11b^{+} cDCs showed a different pattern of *Cx3cr1*-GFP expression, which normally defines a Notch2-dependent GFP^{lo} subset and a GFP^{hi}

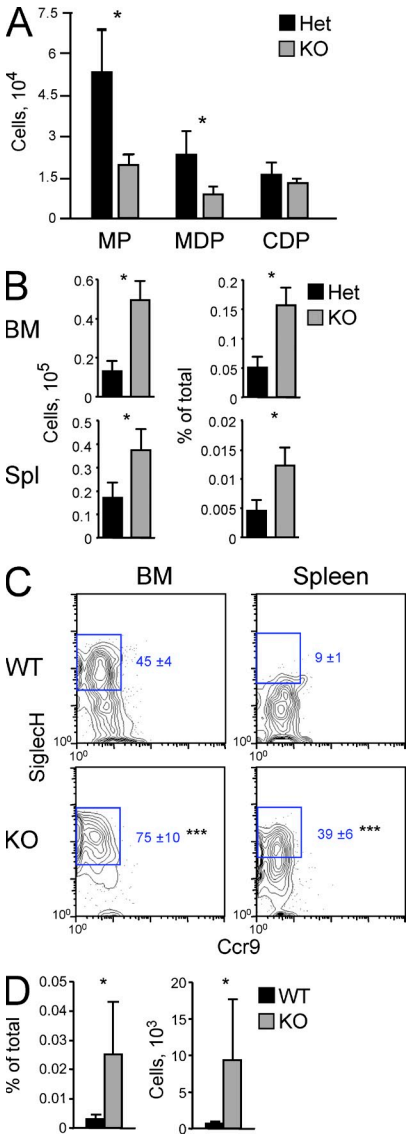

Figure 4. Expansion of SiglecH$^+$ pre-DCs in Mtg16-deficient mice. (A) Early DC progenitors in Mtg16-deficient mice. The BM of heterozygous *Mtg16*$^{+/-}$ (Het) or KO *Mtg16*$^{-/-}$ mice carrying the *Cx3cr1*-GFP reporter was analyzed for the number of the indicated progenitors defined as in Fig. S2 (mean ± SD of five to seven animals pooled from three experiments). MDP, monocyte/DC progenitor. (B) The total pre-DC population in Mtg16-deficient mice. Het or KO mice were analyzed for the fraction and number of Lin$^-$ CD11c$^+$ MHC II$^-$ Flt3$^+$ Sirpα^{lo} pre-DC population in the BM and spleen (mean ± SD of five to seven animals pooled from three experiments). (C) The SiglecH$^+$ pre-DC subset in the WT and *Mtg16*$^{-/-}$ KO animals. Shown are representative staining profiles of pre-DCs gated as in Fig. S2, with the fraction of SiglecH$^+$ subset among pre-DCs indicated (mean ± SD of three to five animals pooled from two experiments). (D) The fraction among total cells and absolute number of SiglecH$^+$ pre-DCs in the spleens of WT and KO mice (mean ± SD of three to five animals pooled from two experiments). *, P ≤ 0.05; ***, P ≤ 0.0005.

subset that resembles monocytes (Lewis et al., 2011). Whereas the proportions of these two populations were unchanged in *Mtg16*$^{-/-}$ spleens, the GFP^{lo} subset had lower levels of GFP, and a novel GFP$^-$ population was apparent (Fig. 3 D). Although the significance of these changes is unclear, they may indicate enhanced differentiation of Notch2-dependent DCs from pre-DCs.

We asked whether the enhanced differentiation of cDCs at the expense of pDCs originates in DC progenitors. Using the *Cx3cr1*-GFP reporter to define early DC progenitors (Fig. S2), we found that MPs and monocyte/DC progenitors were reduced in *Mtg16*$^{-/-}$ BM, whereas CDPs were unchanged (Fig. 4 A). In contrast, the population of MHC II$^-$ Flt3$^+$ Sirpα^{lo} CD11c^{lo} pre-DCs as originally defined by Naik et al. (2006) and Liu et al. (2009) was increased in the BM and spleen (Fig. 4 B). A recent analysis of pre-DCs in the BM revealed their substantial heterogeneity, such as the expression of pDC marker SiglecH and the retention of pDC potential in a fraction of pre-DCs (Satpathy et al., 2012a). We used pDC marker Bst2 to rigorously exclude pDCs from the pre-DC population, which was then further resolved using SiglecH and an early pDC marker Ccr9. Similar to Satpathy et al. (2012a), we found that WT BM pre-DCs contained a large fraction of Ccr9$^-$ SiglecH$^+$ cells, which could give rise to both cDCs and pDCs in Flt3L-supplemented culture (Fig. S2). This pre-DC subset was virtually absent in the WT spleen (Fig. S2), consistent with the terminal cDC commitment of splenic pre-DCs. Notably, the SiglecH$^+$ subset comprised the majority of pre-DCs in *Mtg16*$^{-/-}$ BM, and its fraction and number were strongly increased in *Mtg16*$^{-/-}$ spleen (Fig. 4, C and D). These data suggest that Mtg16 deficiency promotes the development of SiglecH$^+$ pre-DCs and possibly their exit to the periphery, where they are likely to undergo differentiation toward cDCs.

Mtg16 represses Id2 expression in pDCs and in DC progenitors

To explore the mechanism of Mtg16 activity in pDC development, we compared genome-wide expression profiles of pDCs from the BM of *Mtg16*$^{-/-}$ and control mice (Dataset S1). We found that Id2 was among the top differentially expressed genes, ranking as the #7 up-regulated gene in Mtg16-deficient pDCs (Fig. 5 A and Dataset S1). A nearly 10-fold higher level of *Id2* expression in the bulk *Mtg16*$^{-/-}$ pDC population was confirmed by quantitative RT-PCR (qRT-PCR; Fig. 5 B). To analyze the expression of *Id2* at the single-cell level, we used a reporter strain in which a cell surface marker (human CD5 [hCD5]) had been inserted into the 3′ UTR of the *Id2* locus (Jones-Mason et al., 2012). In control reporter mice, pDCs were hCD5 negative, whereas *Mtg16*$^{-/-}$ pDCs uniformly expressed hCD5 (Fig. 5 C).

To analyze the cell type specificity of Id2 induction, we first established the pattern of *Id2*-hCD5 expression. Consistent with the essential role of Id2 in CD8$^+$ cDCs and NK cells, the *Id2*-hCD5 reporter was expressed at the highest level in these cell types (Fig. 5 D). It was also expressed in other lineages including T cells and monocytes, but was absent from pDCs and B cells (Fig. 5 D). In contrast to the induction of hCD5 in Mtg16-null pDCs, other cell types did not show consistent changes in hCD5 expression (Fig. 5 E). Reflecting the loss of pDC-related CD8$^+$ cDC population (Fig. 3 D), the CD5^{lo}

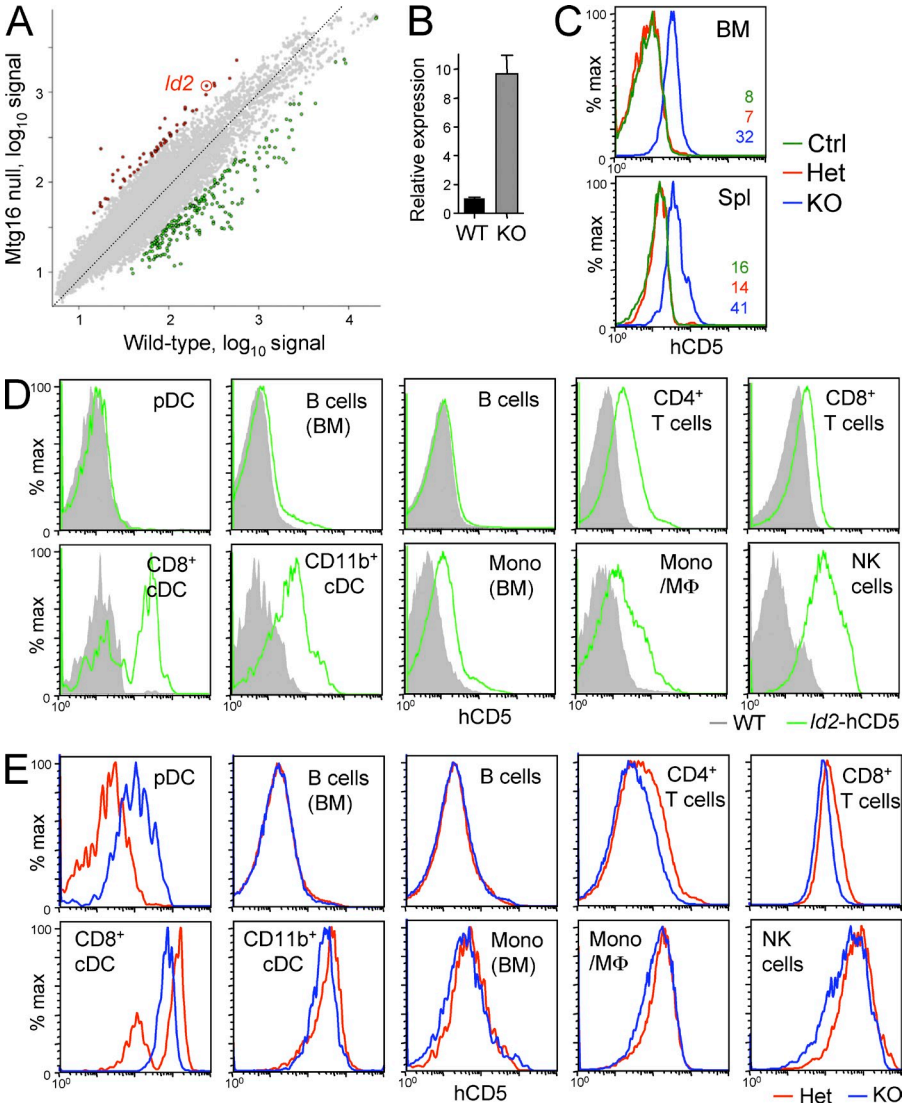

Figure 5. The induction of *Id2* expression in Mtg16-deficient pDCs. (A) Sorted BM pDCs from WT and *Mtg16*$^{-/-}$ mice were analyzed by expression microarray. Shown is pairwise comparison of $\log_{10}$-transformed hybridization signals for individual genes, with the genes overexpressed more than threefold in WT or Mtg16-null pDCs shown in green and red, respectively (results from one experiment). (B) qRT-PCR analysis of *Id2* expression in sorted BM pDCs from WT and *Mtg16*$^{-/-}$ mice (mean ± SD of triplicate PCR reactions). Results are from one experiment representative of two independent sorting experiments and distinct from the one used for microarray. (C) The expression of *Id2* reporter in Mtg16-deficient pDCs. Shown is the surface expression of hCD5 in gated BM and splenic pDCs from *Mtg16*$^{+/-}$ (Het) or *Mtg16*$^{-/-}$ (KO) mice crossed to the *Id2*-hCD5 reporter, as well as from control reporter-negative mice (Ctrl). Results are from one animal per genotype, representative of four independently analyzed animals. (D) The expression pattern of the *Id2*-hCD5 reporter in the immune system. Spleen or BM cells from control WT or *Id2*-hCD5 animals were stained for hCD5. Shown are histograms of hCD5 expression in the indicated gated populations of splenocytes or (where indicated) BM cells. Results are from one animal per genotype, representative of five independently analyzed animals. (E) The expression of *Id2* reporter in the same cell types from *Id2*-hCD5 reporter mice that were heterozygous (Het) or null (KO) for *Mtg16*. Results are from one animal per genotype, representative of three independently analyzed animals.

CD8$^+$ cDCs corresponding to this population were absent from *Mtg16*$^{-/-}$ spleens (Fig. 5 E). Thus, the loss of Mtg16 causes the aberrant induction of *Id2* transcription specifically in pDCs.

We analyzed the stage of Id2 induction during DC development in *Mtg16*$^{-/-}$ animals. No hCD5 expression was detected in WT BM progenitors including long-term HSCs, Flt3$^+$ multipotent progenitors, MPs, and DC progenitors including canonical (CD115$^+$) and putative pDC-biased (CD115$^-$) CDPs (Fig. 6 A). Furthermore, no induction of *Id2* was observed in any of these early progenitors in *Mtg16*$^{-/-}$ BM. In contrast, *Mtg16*$^{-/-}$ pre-DCs (Lin$^-$ MHC II$^-$ B220$^-$ Sirpa^{lo} Flt3$^+$ CD11c^{lo}) showed an induction of *Id2* expression, both in the BM and particularly in the spleen (Fig. 6 B). The strong induction of *Id2* was also detected by qRT-PCR in the Ccr9$^-$ SiglecH$^+$ fraction of pre-DCs from the BM and spleen of Mtg16-deficient mice (Fig. 6 C). Conversely, the expression of E2-2 was decreased approximately twofold, consistent with impaired pDC potential. Thus, the loss of Mtg16 leads to precocious induction of *Id2* in pre-DCs, which is consistent with the enhanced differentiation of the CD8$^+$ cDC subset.

Mtg16 forms a complex with E2-2 and is recruited to the Id2 locus

We analyzed the mechanism of Mtg16 activity in pDCs using human pDC lymphoma cell lines, which recapitulate the expression program and function of pDCs (Chaperot et al., 2006; Karrich et al., 2012). Because ETO proteins are known to associate with E proteins, we tested whether MTG16 interacts with E2-2, the predominant E protein in pDCs. Both MTG16 and E2-2 were expressed in the human pDC cell line Gen2.2 but not in T cell lymphoma MOLT-4 (Fig. 7 A). Immunoprecipitation of Mtg16 from Gen2.2 cells revealed its association with endogenous E2-2 (Fig. 7 A). E proteins including HEB and E2-2 (Sepp et al., 2011) comprise two isoforms, of which only the long isoform is capable of binding ETO proteins (Guo et al., 2009). Only the long isoform of E2-2 was found

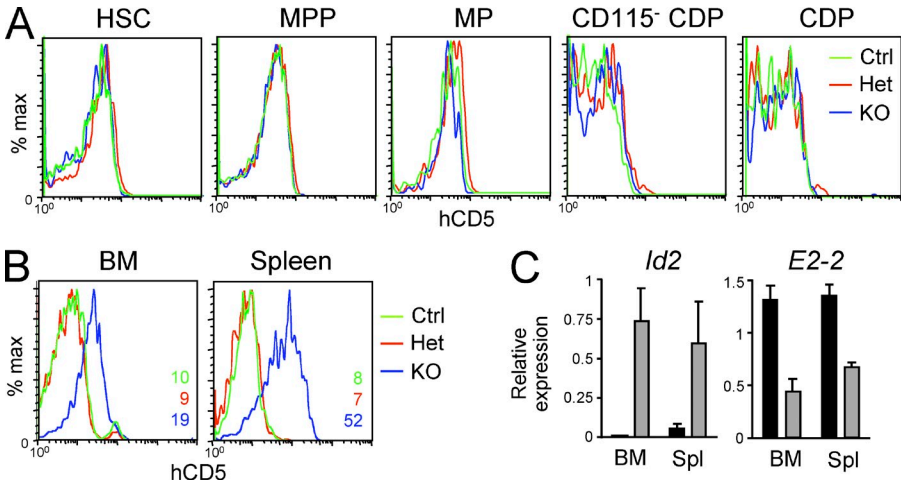

Figure 6. The expression of Id2 commences in Mtg16-deficient DC progenitors. (A and B) The expression of *Id2*-hCD5 reporter in progenitor cell populations, shown as in Fig. 5 C. Shown are staining profiles in the indicated early progenitors in the BM (A) and in pre-DCs in the BM and spleen (B). HSC, Lin^- $Sca1^+$ $c\text{-}Kit^+$ $Flt3^-$; multipotent progenitor (MPP), Lin^- $Sca1^+$ $c\text{-}Kit^+$ $Flt3^+$; MP, Lin^- $Sca1^-$ $c\text{-}Kit^+$ $Flt3^+$; CDP, Lin^- $Sca1^+$ $c\text{-}Kit^{lo}$ $Flt3^+$, $CD115^+$ or $CD115^-$ as indicated. Results are from one animal per genotype, representative of three independently analyzed animals. (C) The expression of indicated genes was tested by qRT-PCR in the $SiglecH^+$ $Ccr9^-$ subset of pre-DCs sorted from pooled BM or spleens of WT or *Mtg16*$^{-/-}$ (KO) animals (mean ± SD of triplicate PCR reactions). Results are from one experiment representative of two experiments.

associated with endogenous MTG16, further confirming the binding specificity (Fig. 7 A).

To analyze the binding of Mtg16 to chromatin in pDCs, we performed parallel chromatin immunoprecipitation (ChIP) followed by sequencing (ChIP-Seq) of MTG16 and E2-2 in the human pDC cell line CAL-1. The promoter of *MTG16* (*CBFA2T3*) itself is a target of binding by Mtg16 (Soler et al., 2010) and indeed was among the top MTG16-binding targets in CAL-1 (Fig. 7 B and Dataset S2). Consistent with the lack of direct DNA binding, MTG16 ChIP yielded lower chromatin enrichment and fewer binding peaks than E2-2 ChIP (Dataset S2). Strikingly, however, 2,050 out of 2,332 MTG16-bound genes (88.8%) were also occupied by E2-2, and 1,692 (82.5%) of those common genes harbored exactly coinciding peaks of MTG16 and E2-2 binding (Dataset S1). The coincident binding of MTG16 and E2-2 was observed on all top targets of MTG16 such as *CBFA2T3* (Fig. 7 A). It was also observed on pDC-enriched targets of E2-2 (Ghosh et al., 2010), including *PTCRA*, *TLR9*, and *PACSIN1* (Fig. 7 C), suggesting that MTG16 is a general cofactor rather than a specific corepressor of E2-2.

To analyze sequence specificity of DNA binding, we used a biophysically motivated, position-specific affinity matrix (PSAM) approach that is equal or superior to other approaches for motif discovery in ChIP data (Weirauch et al., 2013). The analysis of E2-2 peaks using the PSAM-based algorithm MatrixREDUCE revealed a single major sequence motif (CAgcTG) consistent with the canonical E box (Fig. 7 D). The same sequence also represented the top motif in MTG16-bound ChIP peaks in CAL-1 cells, but not in mouse erythroleukemia cells (not depicted; Soler et al., 2010). To further test the overlapping binding preferences of E2-2 and MTG16 in CAL-1, we used the defined E2-2 motif to predict the binding of MTG16 to DNA. The prediction ability of the motif can be quantified by the regression coefficient ("slope") of the underlying linear model. We found that the E2-2 motif was highly predictive not only of E2-2 but also of MTG16 binding (p-value $<10^{-16}$) in CAL-1 cells (Fig. 7 E). These data demonstrate that MTG16 recapitulates the binding specificity of E2-2, suggesting that it is recruited to DNA predominantly through E2-2 in pDCs.

The ChIP-Seq analysis revealed strong peaks for both MTG16 and E2-2 enrichment at ∼105 and ∼135 kb 5′ of *ID2* (Fig. 7 F). This region has no adjacent genes other than *ID2* but was recently shown to contain multiple enhancers, including those specific for cDCs or monocytes (Andersson et al., 2014). We also observed a minor MTG16 peak coinciding with a prominent E2-2 peak within ∼5 kb of the *ID2* promoter region. The binding of the *ID2* promoter-proximal regions by MTG16 and E2-2 was confirmed by qPCR analysis of unamplified ChIP material (Fig. 7 G). Although the function of the distal or proximal MTG16–E2-2–binding sites in *ID2* repression remains to be clarified, these data reveal the recruitment of both proteins to the *ID2* locus in pDCs. Together with the reported role of E2-2 in Id2 repression (Ghosh et al., 2010), they suggest that the MTG16–E2-2 complex binds to and represses the *ID2* locus in pDCs.

The deletion of Id2 facilitates the development of Mtg16-deficient pDCs

To confirm that de-repression of *Id2* contributes to the impaired pDC development in Mtg16-deficient animals, we tested whether it could be rescued by Id2 deficiency. Because Id2-deficient mice die perinatally on C57BL/6 background, we intercrossed *Mtg16*$^{-/-}$ *Id2*$^{+/-}$ animals to obtain *Mtg16*$^{-/-}$ *Id2*$^{-/-}$ or *Mtg16*$^{-/-}$ *Id2*$^{+/+}$ littermate embryos. Intercrosses of WT animals produced control *Mtg16*$^{+/+}$ embryos. Hematopoietic reconstitution of adult recipients with *Mtg16*$^{-/-}$ fetal livers (FLs) was inefficient (not depicted), reflecting the defective function of Mtg16-null HSCs (Fischer et al., 2012). We therefore analyzed pDC development in the embryo, which commences early during definitive hematopoiesis (Dakic et al., 2004). The pDC population could be detected with specific markers in the FLs of WT

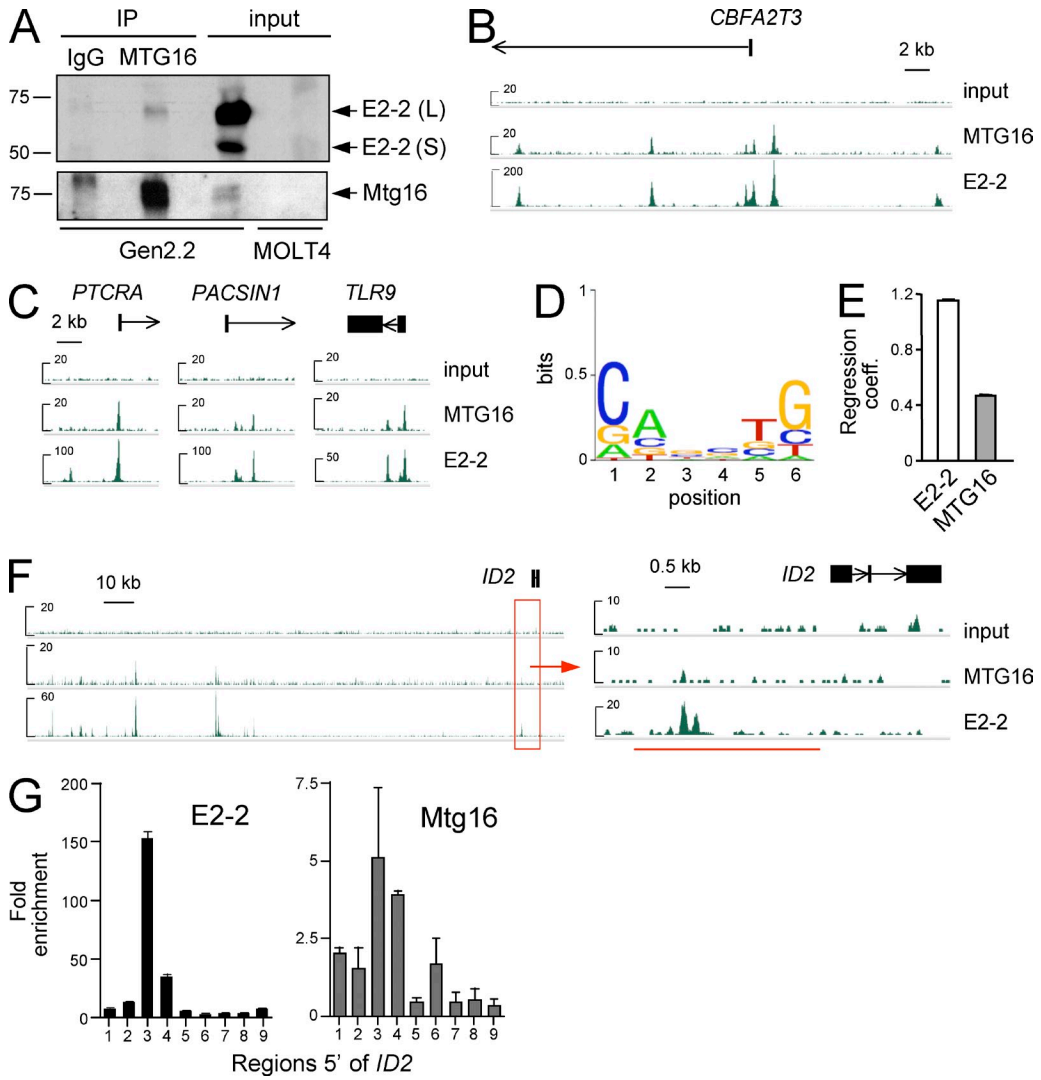

Figure 7. Mtg16 is recruited to chromatin through E2-2 and is enriched at the *ID2* locus in pDCs. (A) Coimmunoprecipitation of endogenous E2-2 and MTG16 in the human pDC cell line Gen2.2. Shown are E2-2 and MTG16 immunoblots of Gen2.2 cell lysates immunoprecipitated (IP) with control IgG or anti-MTG16 antibodies or total input from Gen2.2 or a control non-pDC cell line MOLT-4. Molecular mass markers (kilodaltons) and the long (L) and short (S) isoforms of E2-2 are indicated. Representative of two experiments; the same results were obtained in another pDC cell line, CAL-1 (not depicted). (B) Chromatin enrichment peaks at the *CBFA2T3* (*MTG16*) locus after ChIP-Seq for MTG16 and E2-2 from human pDC cell line CAL-1. Shown are the signal tracks for the total chromatin input, MTG16, and E2-2 ChIP. (C) Chromatin enrichment peaks of MTG16 and E2-2 at the promoters of pDC-enriched genes, as shown in B. (D) A consensus sequence motif of ChIP-Seq peaks of E2-2 in CAL-1 cells, with the "height" of each base corresponding to its frequency at a given position. (E) Regression coefficients of the linear model that predicts the binding of E2-2 or MTG16 according to the motif in D (mean ± SEM of $>10^5$ events). (F) Chromatin enrichment peaks of MTG16 and E2-2 at the *ID2* locus in the human pDC cell line CAL-1. ChIP signals are shown across ~180 kb of the locus and zoomed across ~10 kb of its 5′ region. (G) qPCR analysis of MTG16 and E2-2 binding to the *ID2* promoter in CAL-1. Unamplified chromatin from MTG16 and E2-2 ChIP was analyzed by qPCR with nine primers evenly spanning the ~4-kb region 5′ of *ID2* (red underline in F). Results represent mean ± SD of triplicate PCR reactions from a single experiment; enrichment of the fragment #3 has been confirmed in an independent experiment and also observed in pDC cell line Gen2.2.

embryos (Fig. 8 A). The fraction of pDCs was reduced approximately twofold in *Mtg16*$^{-/-}$ FLs but increased several-fold in *Mtg16*$^{-/-}$ FLs that were also deficient for *Id2* (Fig. 8, A and B). The changes in phenotypic pDC population were reflected in CpG-induced IFN-α secretion by cultured FL cells, which was significantly increased in *Mtg16*$^{-/-}$ *Id2*$^{-/-}$ FL (Fig. 8 C). Furthermore, the reduced Bst2 levels on *Mtg16*$^{-/-}$ pDCs were increased by Id2 deletion (Fig. 8 D), although the levels of other markers were not affected consistently (not depicted). Thus, concomitant loss of Id2 facilitates the development and function of Mtg16-deficient pDCs, suggesting that Id2 induction contributes to their abnormal development.

DISCUSSION

Our analysis of Mtg16-deficient mice revealed reduced numbers, aberrant surface phenotype, and impaired function of

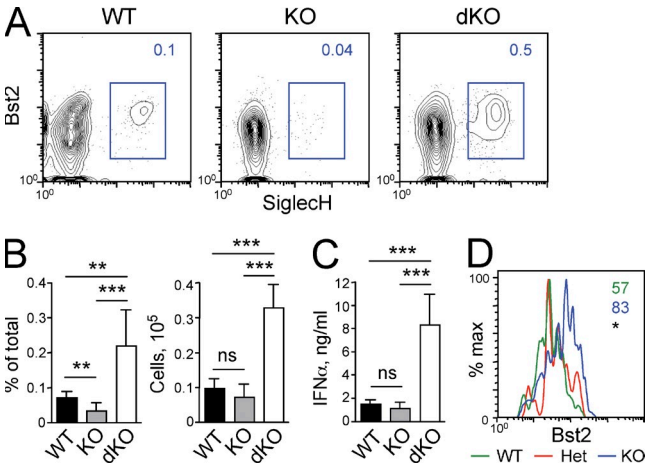

Figure 8. Id2 deletion facilitates the development of Mtg16-deficient pDCs. (A) The pDC population in the FLs of WT, Mtg16-deficient (KO), or Mtg16/Id2 double-deficient (dKO) embryos. Shown are representative staining profiles of gated CD11c$^+$ cells, with the SiglecH$^+$ Bst2$^+$ pDC population and its fraction among total cells indicated. (B) The frequency among total liver cells and absolute numbers of pDCs in the embryos in A (mean ± SD of six to eight embryos per genotype pooled from two to three litters). Significance of pairwise comparisons between samples is indicated (ns, not significant). (C) IFN-α production by FL cells of the indicated genotypes. Total liver cell suspensions were cultured with CpG, and IFN-α in the supernatants was measured by ELISA (mean ± SD of four to seven embryos per genotype pooled from one to two litters). (D) The expression of Bst2 by pDCs from *Mtg16*$^{-/-}$ embryos that were WT (*Id2*$^{+/+}$), heterozygous (Het, *Id2*$^{+/-}$), or null (KO, *Id2*$^{-/-}$) for Id2. The MFIs represent mean values of four to five embryos per genotype pooled from two litters. *, P ≤ 0.05; **, P ≤ 0.005; ***, P ≤ 0.0005.

pDCs, collectively resulting in a failure of pDC-dependent IFN response in vivo. In contrast, Mtg16 deletion caused an expansion of cDC progenitors (pre-DCs) and of the canonical CD8$^+$ cDC subset. Unlike other known regulators of DC development (Satpathy et al., 2012b), the loss of Mtg16 changed DC lineage allocation and enhanced one subset development at the expense of another. These data provide strong genetic evidence for a common developmental pathway of DC development and for the affiliation of pDCs with the DC lineage despite their many lymphoid features (Reizis et al., 2011b). Our data suggest that Mtg16 acts as a molecular "rheostat" that facilitates pDC development and restricts the CD8$^+$ cDC population, whose expansion may be detrimental for antibacterial immunity (Sathaliyawala et al., 2010).

The development of pDCs requires E protein E2-2, whereas its antagonist Id2 is expressed in cDCs and is required for CD8$^+$ cDC development. Notably, Id2 is expressed in most immune cell types but is specifically excluded from pDCs and B cells, the two lineages with high E protein activity conferred by E2-2 and E2a, respectively. Thus, the development of pDCs involves both the induction of E2-2 and the repression of Id2, although the mechanisms of either event remained unclear. We found that Mtg16 deletion caused de-repression of Id2 in pDCs, effectively reducing the net E protein activity in these cells. Indeed, many features of pDCs in *Mtg16*$^{-/-}$ mice resembled those in *E2-2*$^{+/-}$ mice (Cisse et al., 2008), including reduced pDC numbers, decreased levels of certain pDC markers (Ccr9, CD4), and impaired IFN production capacity. In addition, *Mtg16*$^{-/-}$ mice lacked the *Cx3cr1*-GFP$^+$ CD8$^+$ cDC population, whose development depends on E2-2 (Bar-On et al., 2010). Defective pDC development in *Mtg16*$^{-/-}$ embryos was enhanced by Id2 deletion, suggesting a genetic interaction between Mtg16 and Id2. Similarly, Id2 was induced in pre-DCs, likely facilitating their differentiation toward the Id2-dependent CD8$^+$ subset. Collectively, these results suggest that Mtg16 controls subset allocation during DC development in part by repressing Id2 expression and thereby enhancing E protein activity.

The roles of Mtg16 in facilitating pDC development and restricting cDC development might be explained either by independent activities of Mtg16 in committed pDC and cDC progenitors or by a rheostat function in a single common progenitor. Although the former possibility cannot be excluded, our data favor the latter scenario. In particular, the SiglecH$^+$ subset of pre-DCs (Satpathy et al., 2012a) may represent a transition stage between CDPs and fully committed pre-DCs, and as such retain both pDC and cDC potential (at least in vitro). Importantly, this pre-DC subset showed the induction of Id2 in the Mtg16-deficient BM and elevated cell numbers in Mtg16-deficient spleen. It is therefore likely that pre-DCs with elevated Id2 levels undergo precocious cDC commitment, exit into the periphery, expand, and differentiate into CD8$^+$ cDCs. It has been demonstrated that DC potentials can be predetermined at early stages of hematopoiesis (Naik et al., 2013), emphasizing the progressive restriction of lineage potentials in DC progenitors. Our results suggest that Mtg16 represents a cell-intrinsic factor that restricts the cDC potential at late CDP/early pre-DC stage in the BM.

ETO proteins in general and Mtg16 in particular can interact with multiple transcription factors including E proteins (Zhang et al., 2004), Notch receptor intracellular domains (Hunt et al., 2011), and a GATA/SCL/LMO-containing complex (Soler et al., 2010). Our ChIP data suggest that in pDCs, Mtg16 is recruited to chromatin primarily through the E protein E2-2. Notably, Mtg16 was recruited even to the genes activated by E2-2, despite the proposed role of ETO proteins as inhibitors of E protein–mediated transcriptional activation (Zhang et al., 2004; Guo et al., 2009). Therefore, ETO proteins may represent general components of chromatin-bound E protein complexes, whereas additional factors determine the effect of these complexes on target gene activation or repression. Importantly, Mtg16 and E2-2 are jointly bound to the *ID2* locus in pDCs, and the deletion of Mtg16 (this study) and of E2-2 (Ghosh et al., 2010) causes the induction of Id2 in these cells. Although the induction of the Id gene expression by an E protein has been described in invertebrates (Bhattacharya and Baker, 2011), the repression has not been observed previously. Thus, the DC lineage commitment involves a positive feedback mechanism whereby E proteins directly repress the transcription of their inhibitor Id2 through ETO protein corepressors.

Collectively, our results suggest a model whereby ETO protein Mtg16 regulates pDC versus cDC lineage commitment. Uncommitted DC progenitors express low levels of both E2-2 and Id2, with high-level Id2 expression repressed by Mtg16 in complex with E2-2 and possibly other transcription factors. Stochastic or induced up-regulation of E2-2 may facilitate Mtg16-mediated repression of Id2, enhancement of net E protein activity, and pDC commitment. Conversely, up-regulation of Id2 would inhibit E protein activity and thereby dislodge Mtg16 from the *Id2* locus, leading to further up-regulation of Id2 and differentiation along the cDC pathway. Because the deletion of E2-2 causes Id2 up-regulation and spontaneous differentiation into cDCs (Ghosh et al., 2010), the cDC lineage likely represents the "default" pathway of DC differentiation. This scenario describes a mechanism of pDC versus cDC commitment driven by mutually antagonistic transcription factors, a common mechanism of lineage specification in development.

MATERIALS AND METHODS

Animals. All animal experiments were performed according to the investigator's protocol approved by the Institutional Animal Care and Use Committee of Columbia University. *Mtg16*$^{+/-}$ mice (Chyla et al., 2008) on pure C57BL/6 background were intercrossed to generate homo- or heterozygous progeny. Age-matched WT C57BL/6 mice bred in the same animal facility were used as controls; where indicated, heterozygous *Mtg16*$^{+/-}$ mice were used as littermate controls. The Id2-*hCD5* reporter allele (Jones-Mason et al., 2012; provided by Y. Zhuang, Duke University, Durham, NC) and *Cx3cr1*-GFP reporter allele (Jung et al., 2000) on C57BL/6 background were crossed to *Mtg16*$^{+/-}$ mice and used as heterozygotes. The *Id2*-null allele was created by replacing the first exon of *Id2* with a LacZ marker and selection cassette, resulting in a functional null allele as judged by the expected absence of lymph nodes and CD8$^+$ cDCs in homozygous mice. The resulting *Id2*$^{+/-}$ mice were backcrossed to C57BL/6.

For the analysis of *Mtg16*$^{-/-}$ *Id2*$^{-/-}$ embryos, timed matings were performed between *Mtg16*$^{+/-}$ *Id2*$^{+/-}$ and *Mtg16*$^{-/-}$ *Id2*$^{+/-}$ animals, and FLs were isolated for genotyping and analysis on days 17.5–18.5 postcoitum. Matings between WT animals were used to generate control embryos. For competitive hematopoietic reconstitution, BM cells from *Mtg16*$^{-/-}$ or control *Mtg16*$^{+/-}$ mice were mixed with BM cells from C57BL/6 mice congenic for CD45.1 (B6.SJL) at 95:5% ratio and injected i.v. into lethally irradiated B6.SJL recipient mice. For IFN induction in vivo, mice were injected i.v. with 5 mg CpG type A oligonucleotide (ODN 2216; InvivoGen) complexed with DOTAP (Roche; 30 ml DOTAP/150 ml total volume) or with 0.3 mg poly-I:C (GE Healthcare). Serum IFN before injection or 6 (for CpG) or 12 h (for poly-I:C) after injection was measured by ELISA using anti–mouse IFN-α antibodies (PBL Interferon Source).

Cell analysis. Single-cell suspensions were stained for multicolor analysis with the indicated fluorochrome-conjugated antibodies (BD or eBioscience). The samples were acquired on an LSRII flow cytometer or sorted on FACSAria flow sorter (BD) and analyzed with FlowJo software (Tree Star). In all experiments, pDCs were defined by a combination of at least two pDC-enriched markers (CD11c, B220, and/or Ly6C) with at least one pDC-specific marker (Bst2 and/or SiglecH). Lineage-negative cells were defined as CD3$^-$, CD19$^-$, NK1.1$^-$, Ter119$^-$, Ly6G$^-$, B220$^-$. For pDC development in vitro, total BM cells (2×10^6/ml) were cultured for 7 d with 100 ng/ml recombinant human Flt3L (PeproTech). For competitive BM cultures, donor BM cells were mixed 1:1 with B6.SJL BM cells and cultured as above. For the culture of DC progenitors, Lin$^-$ Sca-1$^-$ c-Kit$^{+/lo}$ Flt3$^+$ cells were sorted from pooled BM and cultured with Flt3L as above. To measure IFN production, total cell suspensions or sorted pDCs were incubated for 18 h in the presence of 2 μM CpG type A, and IFN-α in the supernatants was measured by ELISA.

Gene expression analysis. For microarray analysis, BM cells from WT control or *Mtg16*$^{-/-}$ mice were pooled and enriched by negative selection of lineage (CD11b, CD19, DX5, TER119)-negative cells using magnetic microbeads (Miltenyi Biotec). The pDCs (Lin$^-$ CD11c^{int} Bst2$^+$) were sorted directly into TRIzol reagent (Invitrogen), and total RNA was reverse transcribed, amplified, labeled, and hybridized to Mouse Genome 1.0 ST arrays (Affymetrix). The results were gcRMA-normalized by the manufacturer's software and analyzed using the NIA Array software. For qRT-PCR analysis, RNA from a separately sorted pDC sample was reverse transcribed and assayed by SYBR Green-based real-time PCR. The expression of the *Id2* was normalized to that of β-actin and expressed relative to the WT sample via the $\Delta\Delta C_T$ method.

Cell lines, protein analysis, and ChIP. Human pDC lymphoma cell lines CAL-1 (Maeda et al., 2005) and Gen2.2 (Chaperot et al., 2006) and a control human T cell lymphoma MOLT-4 were maintained in complete RPMI medium with 10% FCS under regular tissue culture conditions. For coimmunoprecipitation, Gen2.2 and MOLT-4 cells were lysed using RIPA buffer, and ∼1 mg of whole cell lysate was subjected to immunoprecipitation with anti-Mtg16 polyclonal antibody (C-20; Santa Cruz Biotechnology, Inc.) or IgG control using protein G–agarose beads. The resulting samples were analyzed by Western blotting using anti-Mtg16 antibody or anti–E2-2 monoclonal antibody (clone 367.2; Santa Cruz Biotechnology, Inc.).

For ChIP, CAL-1 cells were cross-linked with formaldehyde for 10 min, sonicated to yield chromatin fragments of ∼200 bp, and subjected to immunoprecipitation with anti-Mtg16 polyclonal antibody or IgG control. E2-2 was immunoprecipitated using a newly developed rabbit monoclonal antibody that recognizes human E2-2 but not related E protiens E2a or HEB. After cross-link reversal, the isolated chromatin was analyzed by qPCR for the indicated ∼5-kb region of *ID2*. The enrichment was normalized to 10% of total chromatin input of the respective sample and expressed as fold enrichment relative to control IgG sample.

ChIP-Seq. Isolated chromatin samples were submitted to the Yale Center for Genome Analysis for amplification, library construction, and sequencing. The samples were sequenced on a single-end version 3 Illumina flow cell on a HiSeq 2000. Sequencing reads were aligned to the human genome (UCSC hg19), and the enrichment peaks were identified, separated, and annotated using the default parameters of MACS 1.4.0 software. Sequence peaks were visualized using DNAnexus genome browser. For motif discovery, we used the BayesPeak algorithm (Spyrou et al., 2009) with a window size set to 100 bp (approximately half of the mean DNA fragment length) to identify 71,326 nonoverlapping peaks with a posterior probability (PP) score of >0.1 in the ChIP-Seq profile for E2-2. MatrixREDUCE (Foat et al., 2006) was used to fit a PSAM ("motif") that optimally explained the variation in PP score across all peaks from the underlying sequence.

Statistical analysis. Statistical significance was estimated with an unpaired, two-tailed Student's *t* test and is indicated as follows: *, $P \le 0.05$; **, $P \le 0.005$; ***, $P \le 0.0005$.

Accession numbers. The ChIP-Seq and microarray data have been deposited in the Gene Expression Omnibus (GEO) database under the accession no. GSE43963.

Online supplemental material. Fig. S1 shows a representative gating strategy to define pDCs in the BM of Mtg16-deficient mice. Fig. S2 characterizes DC progenitors. Dataset S1, included as a separate Excel file, shows genome-wide expression analysis of *Mtg16*$^{-/-}$ pDCs. Dataset S2, included as a separate Excel file, shows ChIP-Seq results for MTG16 and E2-2 in CAL-1 cells. Online supplemental material is available at http://www.jem.org/cgi/content/full/jem.20132121/DC1.

We thank Y. Zhuang for the *Id2* reporter strain, G. Della Gatta, A. Ferrando, and J. Overton for help with ChIP-Seq experiments, and A. Singhee and S. Weisberg for help with ChIP-Seq analysis.

This work was supported by National Institutes of Health (NIH) grant AI072571 and New York State Dept. of Health grant N09G-22 (to B. Reizis), an American Society of Hematology Postdoctoral Fellowship (to H.S. Ghosh), NIH grants AI101251 and AR044535 and the Dana Foundation Neuroimmunology grant (to K. Liu), and NIH grants HG003008 and CA121852 (to H.J. Bussemaker).

The authors declare no competing financial interests.

Submitted: 7 October 2013
Accepted: 29 May 2014

REFERENCES

Allman, D., M. Dalod, C. Asselin-Paturel, T. Delale, S.H. Robbins, G. Trinchieri, C.A. Biron, P. Kastner, and S. Chan. 2006. Ikaros is required for plasmacytoid dendritic cell differentiation. *Blood*. 108:4025–4034. http://dx.doi.org/10.1182/blood-2006-03-007757

Andersson, R., C. Gebhard, I. Miguel-Escalada, I. Hoof, J. Bornholdt, M. Boyd, Y. Chen, X. Zhao, C. Schmidl, T. Suzuki, et al. FANTOM Consortium. 2014. An atlas of active enhancers across human cell types and tissues. *Nature*. 507:455–461. http://dx.doi.org/10.1038/nature12787

Asselin-Paturel, C., G. Brizard, K. Chemin, A. Boonstra, A. O'Garra, A. Vicari, and G. Trinchieri. 2005. Type I interferon dependence of plasmacytoid dendritic cell activation and migration. *J. Exp. Med*. 201:1157–1167. http://dx.doi.org/10.1084/jem.20041930

Bar-On, L., T. Birnberg, K.L. Lewis, B.T. Edelson, D. Bruder, K. Hildner, J. Buer, K.M. Murphy, B. Reizis, and S. Jung. 2010. CX_3CR1^+ $CD8\alpha^+$ dendritic cells are a steady-state population related to plasmacytoid dendritic cells. *Proc. Natl. Acad. Sci. USA*. 107:14745–14750. http://dx.doi.org/10.1073/pnas.1001562107

Belnoue, E., P. Fontannaz, A.F. Rochat, C. Tougne, A. Bergthaler, P.H. Lambert, D.D. Pinschewer, and C.A. Siegrist. 2013. Functional limitations of plasmacytoid dendritic cells limit type I interferon, T cell responses and virus control in early life. *PLoS ONE*. 8:e85302. http://dx.doi.org/10.1371/journal.pone.0085302

Bhattacharya, A., and N.E. Baker. 2011. A network of broadly expressed HLH genes regulates tissue-specific cell fates. *Cell*. 147:881–892. http://dx.doi.org/10.1016/j.cell.2011.08.055

Boos, M.D., Y. Yokota, G. Eberl, and B.L. Kee. 2007. Mature natural killer cell and lymphoid tissue-inducing cell development requires Id2-mediated suppression of E protein activity. *J. Exp. Med*. 204:1119–1130. http://dx.doi.org/10.1084/jem.20061959

Chaperot, L., A. Blum, O. Manches, G. Lui, J. Angel, J.P. Molens, and J. Plumas. 2006. Virus or TLR agonists induce TRAIL-mediated cytotoxic activity of plasmacytoid dendritic cells. *J. Immunol*. 176:248–255. http://dx.doi.org/10.4049/jimmunol.176.1.248

Chyla, B.J., I. Moreno-Miralles, M.A. Steapleton, M.A. Thompson, S. Bhaskara, M. Engel, and S.W. Hiebert. 2008. Deletion of Mtg16, a target of t(16;21), alters hematopoietic progenitor cell proliferation and lineage allocation. *Mol. Cell. Biol*. 28:6234–6247. http://dx.doi.org/10.1128/MCB.00404-08

Cisse, B., M.L. Caton, M. Lehner, T. Maeda, S. Scheu, R. Locksley, D. Holmberg, C. Zweier, N.S. den Hollander, S.G. Kant, et al. 2008. Transcription factor E2-2 is an essential and specific regulator of plasmacytoid dendritic cell development. *Cell*. 135:37–48. http://dx.doi.org/10.1016/j.cell.2008.09.016

Dakic, A., Q.X. Shao, A. D'Amico, M. O'Keeffe, W.F. Chen, K. Shortman, and L. Wu. 2004. Development of the dendritic cell system during mouse ontogeny. *J. Immunol*. 172:1018–1027. http://dx.doi.org/10.4049/jimmunol.172.2.1018

Fischer, M.A., I. Moreno-Miralles, A. Hunt, B.J. Chyla, and S.W. Hiebert. 2012. Myeloid translocation gene 16 is required for maintenance of haematopoietic stem cell quiescence. *EMBO J.* 31:1494–1505. http://dx.doi.org/10.1038/emboj.2011.500

Foat, B.C., A.V. Morozov, and H.J. Bussemaker. 2006. Statistical mechanical modeling of genome-wide transcription factor occupancy data by MatrixREDUCE. *Bioinformatics*. 22:e141–e149. http://dx.doi.org/10.1093/bioinformatics/btl223

Geissmann, F., M.G. Manz, S. Jung, M.H. Sieweke, M. Merad, and K. Ley. 2010. Development of monocytes, macrophages, and dendritic cells. *Science*. 327:656–661. http://dx.doi.org/10.1126/science.1178331

Ghosh, H.S., B. Cisse, A. Bunin, K.L. Lewis, and B. Reizis. 2010. Continuous expression of the transcription factor e2-2 maintains the cell fate of mature plasmacytoid dendritic cells. *Immunity*. 33:905–916. http://dx.doi.org/10.1016/j.immuni.2010.11.023

Ginhoux, F., K. Liu, J. Helft, M. Bogunovic, M. Greter, D. Hashimoto, J. Price, N. Yin, J. Bromberg, S.A. Lira, et al. 2009. The origin and development of nonlymphoid tissue $CD103^+$ DCs. *J. Exp. Med*. 206:3115–3130. http://dx.doi.org/10.1084/jem.20091756

Guo, C., Q. Hu, C. Yan, and J. Zhang. 2009. Multivalent binding of the ETO corepressor to E proteins facilitates dual repression controls targeting chromatin and the basal transcription machinery. *Mol. Cell. Biol*. 29:2644–2657. http://dx.doi.org/10.1128/MCB.00073-09

Hacker, C., R.D. Kirsch, X.S. Ju, T. Hieronymus, T.C. Gust, C. Kuhl, T. Jorgas, S.M. Kurz, S. Rose-John, Y. Yokota, and M. Zenke. 2003. Transcriptional profiling identifies Id2 function in dendritic cell development. *Nat. Immunol*. 4:380–386. http://dx.doi.org/10.1038/ni903

Haniffa, M., M. Collin, and F. Ginhoux. 2013. Ontogeny and functional specialization of dendritic cells in human and mouse. *Adv. Immunol*. 120:1–49. http://dx.doi.org/10.1016/B978-0-12-417028-5.00001-6

Hunt, A., M. Fischer, M.E. Engel, and S.W. Hiebert. 2011. Mtg16/Eto2 contributes to murine T-cell development. *Mol. Cell. Biol*. 31:2544–2551. http://dx.doi.org/10.1128/MCB.01458-10

Jackson, J.T., Y. Hu, R. Liu, F. Masson, A. D'Amico, S. Carotta, A. Xin, M.J. Camilleri, A.M. Mount, A. Kallies, et al. 2011. Id2 expression delineates differential checkpoints in the genetic program of $CD8\alpha^+$ and $CD103^+$ dendritic cell lineages. *EMBO J.* 30:2690–2704. http://dx.doi.org/10.1038/emboj.2011.163

Jones-Mason, M.E., X. Zhao, D. Kappes, A. Lasorella, A. Iavarone, and Y. Zhuang. 2012. E protein transcription factors are required for the development of $CD4^+$ lineage T cells. *Immunity*. 36:348–361. http://dx.doi.org/10.1016/j.immuni.2012.02.010

Jung, S., J. Aliberti, P. Graemmel, M.J. Sunshine, G.W. Kreutzberg, A. Sher, and D.R. Littman. 2000. Analysis of fractalkine receptor CX_3CR1 function by targeted deletion and green fluorescent protein reporter gene insertion. *Mol. Cell. Biol*. 20:4106–4114. http://dx.doi.org/10.1128/MCB.20.11.4106-4114.2000

Karrich, J.J., M. Balzarolo, H. Schmidlin, M. Libouban, M. Nagasawa, R. Gentek, S. Kamihira, T. Maeda, D. Amsen, M.C. Wolkers, and B. Blom. 2012. The transcription factor Spi-B regulates human plasmacytoid dendritic cell survival through direct induction of the antiapoptotic gene BCL2-A1. *Blood*. 119:5191–5200. http://dx.doi.org/10.1182/blood-2011-07-370239

Kee, B.L. 2009. E and ID proteins branch out. *Nat. Rev. Immunol*. 9:175–184. http://dx.doi.org/10.1038/nri2507

Lewis, K.L., M.L. Caton, M. Bogunovic, M. Greter, L.T. Grajkowska, D. Ng, A. Klinakis, I.F. Charo, S. Jung, J.L. Gommerman, et al. 2011. Notch2 receptor signaling controls functional differentiation of dendritic cells in the spleen and intestine. *Immunity*. 35:780–791. http://dx.doi.org/10.1016/j.immuni.2011.08.013

Liu, K., G.D. Victora, T.A. Schwickert, P. Guermonprez, M.M. Meredith, K. Yao, F.F. Chu, G.J. Randolph, A.Y. Rudensky, and M. Nussenzweig. 2009. In vivo analysis of dendritic cell development and homeostasis. *Science*. 324:392–397.

Liu, Y.J. 2005. IPC: professional type 1 interferon-producing cells and plasmacytoid dendritic cell precursors. *Annu. Rev. Immunol*. 23:275–306. http://dx.doi.org/10.1146/annurev.immunol.23.021704.115633

Maeda, T., K. Murata, T. Fukushima, K. Sugahara, K. Tsuruda, M. Anami, Y. Onimaru, K. Tsukasaki, M. Tomonaga, R. Moriuchi, et al. 2005. A novel plasmacytoid dendritic cell line, CAL-1, established from a patient with blastic natural killer cell lymphoma. *Int. J. Hematol*. 81:148–154. http://dx.doi.org/10.1532/IJH97.04116

Merad, M., P. Sathe, J. Helft, J. Miller, and A. Mortha. 2013. The dendritic cell lineage: ontogeny and function of dendritic cells and their subsets in the steady state and the inflamed setting. *Annu. Rev. Immunol*. 31:563–604. http://dx.doi.org/10.1146/annurev-immunol-020711-074950

Miller, J.C., B.D. Brown, T. Shay, E.L. Gautier, V. Jojic, A. Cohain, G. Pandey, M. Leboeuf, K.G. Elpek, J. Helft, et al. Immunological Genome Consortium. 2012. Deciphering the transcriptional network of the dendritic cell lineage. *Nat. Immunol*. 13:888–899. http://dx.doi.org/10.1038/ni.2370

Murre, C. 2005. Helix-loop-helix proteins and lymphocyte development. *Nat. Immunol.* 6:1079–1086. http://dx.doi.org/10.1038/ni1260

Nagasawa, M., H. Schmidlin, M.G. Hazekamp, R. Schotte, and B. Blom. 2008. Development of human plasmacytoid dendritic cells depends on the combined action of the basic helix-loop-helix factor E2-2 and the Ets factor Spi-B. *Eur. J. Immunol.* 38:2389–2400. http://dx.doi.org/10.1002/eji.200838470

Naik, S.H., A.I. Proietto, N.S. Wilson, A. Dakic, P. Schnorrer, M. Fuchsberger, M.H. Lahoud, M. O'Keeffe, Q.X. Shao, W.F. Chen, et al. 2005. Cutting edge: Generation of splenic $CD8^+$ and $CD8^-$ dendritic cell equivalents in Fms-like tyrosine kinase 3 ligand bone marrow cultures. *J. Immunol.* 174:6592–6597. http://dx.doi.org/10.4049/jimmunol.174.11.6592

Naik, S.H., D. Metcalf, A. van Nieuwenhuijze, I. Wicks, L. Wu, M. O'Keeffe, and K. Shortman. 2006. Intrasplenic steady-state dendritic cell precursors that are distinct from monocytes. *Nat. Immunol.* 7:663–671. http://dx.doi.org/10.1038/ni1340

Naik, S.H., P. Sathe, H.Y. Park, D. Metcalf, A.I. Proietto, A. Dakic, S. Carotta, M. O'Keeffe, M. Bahlo, A. Papenfuss, et al. 2007. Development of plasmacytoid and conventional dendritic cell subtypes from single precursor cells derived in vitro and in vivo. *Nat. Immunol.* 8:1217–1226. http://dx.doi.org/10.1038/ni1522

Naik, S.H., L. Perié, E. Swart, C. Gerlach, N. van Rooij, R.J. de Boer, and T.N. Schumacher. 2013. Diverse and heritable lineage imprinting of early haematopoietic progenitors. *Nature.* 496:229–232. http://dx.doi.org/10.1038/nature12013

Onai, N., A. Obata-Onai, M.A. Schmid, T. Ohteki, D. Jarrossay, and M.G. Manz. 2007. Identification of clonogenic common $Flt3^+$M-$CSFR^+$ plasmacytoid and conventional dendritic cell progenitors in mouse bone marrow. *Nat. Immunol.* 8:1207–1216. http://dx.doi.org/10.1038/ni1518

Onai, N., K. Kurabayashi, M. Hosoi-Amaike, N. Toyama-Sorimachi, K. Matsushima, K. Inaba, and T. Ohteki. 2013. A clonogenic progenitor with prominent plasmacytoid dendritic cell developmental potential. *Immunity.* 38:943–957. http://dx.doi.org/10.1016/j.immuni.2013.04.006

Reizis, B., A. Bunin, H.S. Ghosh, K.L. Lewis, and V. Sisirak. 2011a. Plasmacytoid dendritic cells: recent progress and open questions. *Annu. Rev. Immunol.* 29:163–183. http://dx.doi.org/10.1146/annurev-immunol-031210-101345

Reizis, B., M. Colonna, G. Trinchieri, F. Barrat, and M. Gilliet. 2011b. Plasmacytoid dendritic cells: one-trick ponies or workhorses of the immune system? *Nat. Rev. Immunol.* 11:558–565. http://dx.doi.org/10.1038/nri3027

Sathaliyawala, T., W.E. O'Gorman, M. Greter, M. Bogunovic, V. Konjufca, Z.E. Hou, G.P. Nolan, M.J. Miller, M. Merad, and B. Reizis. 2010. Mammalian target of rapamycin controls dendritic cell development downstream of Flt3 ligand signaling. *Immunity.* 33:597–606. http://dx.doi.org/10.1016/j.immuni.2010.09.012

Sathe, P., D. Vremec, L. Wu, L. Corcoran, and K. Shortman. 2013. Convergent differentiation: myeloid and lymphoid pathways to murine plasmacytoid dendritic cells. *Blood.* 121:11–19. http://dx.doi.org/10.1182/blood-2012-02-413336

Satpathy, A.T., W. Kc, J.C. Albring, B.T. Edelson, N.M. Kretzer, D. Bhattacharya, T.L. Murphy, and K.M. Murphy. 2012a. Zbtb46 expression distinguishes classical dendritic cells and their committed progenitors from other immune lineages. *J. Exp. Med.* 209:1135–1152. http://dx.doi.org/10.1084/jem.20120030

Satpathy, A.T., X. Wu, J.C. Albring, and K.M. Murphy. 2012b. Re(de)fining the dendritic cell lineage. *Nat. Immunol.* 13:1145–1154. http://dx.doi.org/10.1038/ni.2467

Sawai, C.M., V. Sisirak, H.S. Ghosh, E.Z. Hou, M. Ceribelli, L.M. Staudt, and B. Reizis. 2013. Transcription factor Runx2 controls the development and migration of plasmacytoid dendritic cells. *J. Exp. Med.* 210:2151–2159. http://dx.doi.org/10.1084/jem.20130443

Sepp, M., K. Kannike, A. Eesmaa, M. Urb, and T. Timmusk. 2011. Functional diversity of human basic helix-loop-helix transcription factor TCF4 isoforms generated by alternative 5′ exon usage and splicing. *PLoS ONE.* 6:e22138. http://dx.doi.org/10.1371/journal.pone.0022138

Soler, E., C. Andrieu-Soler, E. de Boer, J.C. Bryne, S. Thongjuea, R. Stadhouders, R.J. Palstra, M. Stevens, C. Kockx, W. van Ijcken, et al. 2010. The genome-wide dynamics of the binding of Ldb1 complexes during erythroid differentiation. *Genes Dev.* 24:277–289. http://dx.doi.org/10.1101/gad.551810

Spits, H., F. Couwenberg, A.Q. Bakker, K. Weijer, and C.H. Uittenbogaart. 2000. Id2 and Id3 inhibit development of $CD34^+$ stem cells into predendritic cell (pre-DC)2 but not into pre-DC1. Evidence for a lymphoid origin of pre-DC2. *J. Exp. Med.* 192:1775–1784. http://dx.doi.org/10.1084/jem.192.12.1775

Spyrou, C., R. Stark, A.G. Lynch, and S. Tavaré. 2009. BayesPeak: Bayesian analysis of ChIP-seq data. *BMC Bioinformatics.* 10:299. http://dx.doi.org/10.1186/1471-2105-10-299

Steinman, R.M. 2012. Decisions about dendritic cells: past, present, and future. *Annu. Rev. Immunol.* 30:1–22. http://dx.doi.org/10.1146/annurev-immunol-100311-102839

Weirauch, M.T., A. Cote, R. Norel, M. Annala, Y. Zhao, T.R. Riley, J. Saez-Rodriguez, T. Cokelaer, A. Vedenko, S. Talukder, et al. DREAM5 Consortium. 2013. Evaluation of methods for modeling transcription factor sequence specificity. *Nat. Biotechnol.* 31:126–134. http://dx.doi.org/10.1038/nbt.2486

Zhang, J., M. Kalkum, S. Yamamura, B.T. Chait, and R.G. Roeder. 2004. E protein silencing by the leukemogenic AML1-ETO fusion protein. *Science.* 305:1286–1289. http://dx.doi.org/10.1126/science.1097937